RSC Advances

This is an *Accepted Manuscript*, which has been through the Royal Society of Chemistry peer review process and has been accepted for publication.

Accepted Manuscripts are published online shortly after acceptance, before technical editing, formatting and proof reading. Using this free service, authors can make their results available to the community, in citable form, before we publish the edited article. This *Accepted Manuscript* will be replaced by the edited, formatted and paginated article as soon as this is available.

You can find more information about *Accepted Manuscripts* in the Information for Authors.

Please note that technical editing may introduce minor changes to the text and/or graphics, which may alter content. The journal's standard Terms & Conditions and the Ethical guidelines still apply. In no event shall the Royal Society of Chemistry be held responsible for any errors or omissions in this *Accepted Manuscript* or any consequences arising from the use of any information it contains.

ROYAL SOCIETY OF CHEMISTRY

www.rsc.org/advances

Photocatalytic-degradation and reduction of organic compounds using SnO_2 Quantum Dots (via green route) under direct sunlight

Archita Bhattacharjee and M. Ahmaruzzaman*

Department of Chemistry, National Institute of Technology, Silchar-788010, Assam, India

ABSTRACT

SnO_2 Quantum Dots (QDs) were synthesized by a facile and green biological method using sugar cane juice. The biomolecules present in the juice acts as complexing as well as capping agent. No other external agents are required for the production of the SnO_2 Quantum Dots (QDs). This method resulted in the formation of spherical SnO_2 QDs having particle size ~2.5-4.5nm with a tetragonal crystal structure. The biosynthesized SnO_2 QDs were characterized by Transmission electron microscopy (TEM), Selected area electron diffraction (SAED), Energy Dispersive Spectroscopy (EDS) and Fourier transformed infrared spectroscopy (FT-IR). The optical properties were investigated using UV-visible spectroscopy. In the electronic spectra, a clear blue shift in the band gap energy is observed with a decrease in particle size. This is because of three dimensional quantum confinement effects. The biosynthesized SnO_2 QDs act as an efficient photocatalyst for the degradation of Rose Bengal and Methylene blue dye under direct sunlight. The catalytic activity of the biosynthesized SnO_2 QDs were also evaluated by the conversion of p-nitrophenol to p-aminophenol in presence of $NaBH_4$. The reaction was carried out in a green solvent i.e., water at room temperature. It was observed that 99.5% of p-nitrophenol was reduced in presence of SnO_2 QDs within 60 m. These investigations indicate that the biosynthesized SnO_2 QDs may be effective and potential materials for the elimination of hazardous pollutants from wastewater.

Keywords: SnO_2 QDs, sugar cane juice, catalyst, Rose Bengal, methylene blue, p-nitrophenol.

***Corresponding author:** mda2002@gmail.com; Telephone/Fax Number: +913842-242915/+913842-224797

RSC Advances Accepted Manuscript

1. Introduction

There is a growing research in the field of semiconductor quantum dots because of their novel physical and chemical properties. Among them, wide band gap metal oxide semiconductor quantum dots, such as nanocrystalline SnO_2 have been a subject of investigation in recent years. This is because of their novel functional properties as a result of quantum confinement effect. Tin oxide (SnO_2) is an n-type semiconductor with a wide band gap of 3.6 eV [1]. SnO_2 with a tetragonal crystal structure has potential applications in the field of catalysis, transparent conducting electrodes, rechargeable lithium batteries and opto-electronic device [2-8]. SnO_2 quantum dots showed interesting properties because of high surface-to-volume ratio.

Various methods are used for the synthesis of SnO_2 QDs, such as laser ablation method, wet chemical route and microwave heating method [9-11]. There are numerous physical and chemical methods applied for the synthesis of SnO_2 QDs. Most of these methods required high cost of operation, toxic solvents and chemicals, high temperature, capping agents, and other additives. Therefore, the green approach for the synthesis of SnO_2 nanostructures is gaining more importance. Srivastava et al. [12] synthesized spherical SnO_2 nanoparticles using bacteria. Besides this, there is a new method known as phytosynthesis, has gained much interest because of various advantages over other methods. Phytosynthesis is a facile, cost-effective and green approach for the synthesis of nanostructures. Metal oxide nanostructures synthesized using this method may possess additional medicinal applications, such as drug delivery and biosensors.

This communication illustrates the environmentally benign synthesis of SnO_2 QDs using sugar cane (*Saccharum officinarum*) juice. *Saccharum officinarum* (sugar cane) belongs to the poaceae family. It contains non-reducing and reducing sugars, polysaccharides, oligosaccharides, aminoacids, and organic acids and inorganic salts [13]. The various biomolecules, such as aminoacids and other organic acids,

RSC Advances Accepted Manuscript

present in the sugar cane juice also act as complexing as well as capping agents in the synthesis of SnO_2 nanoparticles. The use of sugar cane juice leads to the formation of SnO_2 QDs.

This article reports microwave assisted facile and green synthesis of SnO_2 QDs. Among various methods, microwave heating method is chosen because of its several advantages, such as short reaction time, good control over particle size and uniform nucleation of powders in suspension.

Industrial effluents lead to serious environmental problems. Dyes are the major organic compounds used in various industries, such as textile industries, dyeing, printing, and cosmetics. These dye effluents were discharged from various industries into the nearby water source without further treatment. Most of the dyes are toxic in nature and their disposals into the environment causes serious health hazards and also possess a threat to our ecosystem. Therefore, it is necessary to remove the dye pollutants from industrial wastewater to reduce water pollution. Photocatalytic degradation of dyes by means of UV or solar irradiation with appropriate photocatalyst is a green and effective method for the treatment of dye molecules. This photodegradation process converts dye molecules into non-hazardous compounds. The nanostructured semiconductor metal-oxides act as a good photocatalyst for the degradation of dyes and proves to be an effective means for the elimination of various water pollutants [14-19]. Among the semiconductor metal-oxides, SnO_2 nanoparticles were identified as one of the effective photocatalyst because of their high surface reactivity, large number of active sites and high absorption power of light radiation [14]. In this article, we report the photocatalytic activity of the biosynthesized SnO_2 QDs for the degradation of Rose Bengal and Methylene blue dye by solar irradiation. Rose Bengal is a hazardous water soluble, halogen-containing, fluorescent dye and has adverse toxic effects [20]. Methylene blue is also a water soluble dye used in pharmaceutical drugs and as a colorant in textile industries. It is toxic and causes anemia, bladder irritation and gastrointestinal problems. Therefore, the removal of such dye

RSC Advances Accepted Manuscript

effluents from water is very necessary for avoiding adverse health hazards and also to prevent our ecosystem.

Among the various organic pollutants, para-nitrophenol is listed as toxic pollutants by the United States Environmental Protection Agency (USEPA) [21]. Hence, the discharge of p-nitrophenol from industries into the nearby water system without any treatment leads to serious environmental problems. Therefore, the removal of p-nitrophenol (PNP) from the wastewater is very much important from the environmental point of view. This paper reports the catalytic hydrogenation of p-nitrophenol to p-aminophenol (PAP) in presence of $NaBH_4$ using biosynthesized SnO_2 QDs as a catalyst. The reaction was carried out in a green solvent i.e., water at room temperature. The p-aminophenol is an important intermediate in the synthesis of various analgesic and antipyretic drugs, such as paracetamol, acetanilide and phenacitin. It has enormous applications in the synthesis of various dyes, as a photographic-developer, and corrosion inhibitor [22]. Hence, the synthesis of PAP from PNP by a cheaper and effective method is always appreciable. The conventional method of hydrogenation of PNP utilizes reagents, such as iron/acid and tin/acid as reducing agents. Such methods are expensive in nature and are also associated with serious environmental problems because of the production of large amount of metal-oxide sludge and corrosion of equipments. Hence, we design the conversion of PNP to PAP using heterogeneous metal-oxide (SnO_2 QDs) nanocatalyst in presence of $NaBH_4$ in aqueous medium.

2. Experimental

2.1. Materials:

Stannous Chloride dihydrate ($SnCl_2.H_2O$) and sodium borohydride ($NaBH_4$) were purchased from Merck. Rose Bengal, Methylene blue and p-nitrophenol were purchased from Hi-media. All the chemicals were of analytical grade and were used without further purification. Deionized water was used for the synthesis of

RSC Advances Accepted Manuscript

SnO_2 nanoparticles. The reaction was carried out in a domestic microwave oven. The sugar cane juice was obtained according to the method discussed below.

2.2. Preparation of Sugar Cane Juice:

Saccharum officinarum (sugar cane) stems were purchased locally and were crushed using a two roller crusher machine to extract the sugar cane juice. The juice was collected and filtered through a Whatmann filter paper no. 41.

2.3. Biosynthesis of SnO_2 Quantum Dots (QDs):

The biosynthesis of SnO_2 QDs was carried out by treating 0.01M $SnCl_2.2H_2O$ with 10% sugar cane solution and the mixture was exposed to microwaves. The mixture was irradiated with thirty 10s shots which lead to the formation of light yellow precipitate. The precipitate was washed repeatedly with ethanol and deionized water to remove unwanted impurities. The final product was calcined at 200^oC and collected for characterization. To check the reproducibility of the results, this experiment was repeated three times under similar conditions. The XRD pattern, TEM and UV-visible spectra were recorded and similar results were obtained.

2.4. Characterization of SnO_2 Quantum Dots:

The crystallinity, particle size and crystal structure of the synthesized SnO_2 QDs were evaluated by powder X-ray diffraction (XRD) method using Phillips X'Pert PRO diffractometer with Cu Kα radiation of wavelength 1.5418Å. The size, morphology and diffraction ring pattern of SnO_2 QDs were determined by JEM-2100 Transmission Electron Microscope at an accelerating voltage of 200 kV. The elemental analysis of nanoparticles was carried out by using an EDS analyzer associated with SEM (JSM-7600F). Infrared spectra were also recorded in the wave number range from 400 to 4000 cm^{-1} by using Bruker Hyperion 3000 FTIR spectrometer. UV-visible absorption spectra of the synthesized SnO_2 QDs were recorded on Cary 100 BIO UV-visible spectrophotometer equipped with 1cm quartz cell.

RSC Advances Accepted Manuscript

2.5. Evaluation of photocatalytic activity of biosynthesized SnO_2 QDs:

The photocatalytic activity of biosynthesized SnO_2 QDs was evaluated by the degradation of two different classes of organic dyes, Rose Bengal (RB) and Methylene blue (MB) under direct sunlight. To evaluate the photocatalytic activity, 10 mg of SnO_2 photocatalyst was dispersed in 200 ml of 10^{-4} M aqueous solution of two different dyes by sonication. The solutions were then exposed to sunlight irradiation. The experiments were carried out on a sunny day at Silchar city between 10a.m–3p.m (outside temperature 35^0-40 ^{0}C). The progress of the reactions was monitored by recording UV-visible spectra at regular interval of time. To check the reproducibility of the results, both the experiments were repeated three times and near about similar results were obtained. Error bars were added to show the triplicate results.

2.6. Catalytic activity of synthesized SnO_2 QDs:

The conversion of p-nitro phenol (PNP) to p-amino phenol (PAP) was carried out using aqueous solution of sodium borohydride at room temperature in presence of SnO_2 QDs as a catalyst. The catalytic reduction of PNP takes place in a standard quartz cuvette of 1cm path length. In the cuvette, 2.6 ml of water and 60 µl of $6.0x10^{-3}$ M PNP were taken separately and the absorbance was recorded using the UV-visible spectrometer. A total of 350µl of 0.1M aqueous solution of $NaBH_4$ was added to the p-nitrophenol present in the cuvette and the absorbance was recorded. Now, 300 µl aqueous solution of SnO_2 QDs (0.01g) was added to the mixture and UV-visible absorption spectra were recorded till the peak due to the presence of nitro group disappeared completely.

3. Results and Discussion

3.1. Characterization of the synthesized SnO_2 QDs:

FT-IR spectrum is recorded in order to detect the formation of SnO_2 QDs (Fig.1a). The peak at 601cm^{-1} is assigned to Sn-O-Sn stretching mode of surface bridging oxide formed by the condensation of adjacent hydroxyl groups [23]. The band around 3425 cm^{-1} indicates the presence of O-H group. This band is

RSC Advances Accepted Manuscript

assigned to water molecules present on the surface of SnO_2 nanoparticles and also to stretching vibrations of Sn–OH groups [23]. Therefore, the presence of these bands confirmed the formation of SnO_2. FT-IR spectrum is recorded not only to detect the formation of SnO_2 quantum dots but also to perceive the existence of capping agents adsorbed on the surface of SnO_2 quantum dots. A sharp peak observed at 1631cm^{-1} is attributed to C=O stretch of amide of aminoacids present in protein moiety or other biomolecules containing -COO group (such as various organic acids, monosaccharides etc.) present in the sugar cane juice [12]. The presence of the band around 1012 cm^{-1} is due to C-O stretching vibration of monosaccharides and polysaccharides present in sugar cane juice [24]. These bands indicate that biomolecules present in the sugar cane juice got adsorbed on the surface of SnO_2 quantum dots and therefore, act as a good capping agent in the synthesis of SnO_2 QDs.

The optical properties of biosynthesized SnO_2 QDs were explored by recording the absorption spectrum. Absorption spectrum is also recorded in order to perceive the band gap energy of the biosynthesized SnO_2 QDs. Fig. 1(b) represents the absorption spectrum of biosynthesized SnO_2 QDs. 0.01M solution of SnO_2 QDs was prepared for recording the absorption spectra. The optical properties of semiconductor nanoparticles are strongly particle size dependent. From the spectra, it is evident that the absorption onset shows a blue shift with a decrease in grain size. The observed blue shift of absorption onset is the direct consequence of quantum confinement effect which is associated with smaller particle size. Due to this quantum confinement effect, the band gap of the particle increases as the particle size decreases and results in the shift of absorption onset to lower wavelength. Therefore, quantum confinement effect plays an important role in determining the optical properties of semiconductor nanoparticles.

From the absorption spectra direct band gap energy is calculated using Tauc relation:

$$\alpha(\nu)\, h\nu = K\,(h\nu - E_g)^n \quad \text{---------- (1)}$$

RSC Advances Accepted Manuscript

where, α(ν) is absorption coefficient, K is a constant, E_g is the band gap energy, hν is the incident photon energy and the exponent 'n' equals to ½ for direct band gap semiconductor. Hence, from the plot of $(\alpha h\nu)^2$ versus hν and extrapolation of the linear region of the curve to zero absorption coefficient, optical band gap energy (E_g) can be obtained [23]. Fig. 1(c) graphically represents the plot of $(\alpha h\nu)^2$ versus hν for the biosynthesized SnO_2 QDs. An extrapolation of the linear region of the curve gives the value of optical band gap and is found to be 4.1eV. The band gap energy of biosynthesized SnO_2 QDs was found to be greater than the reported value of bulk SnO_2 (3.6 eV). Hence, a clear blue shift in band gap energy is observed with a decrease in grain size. This blue shift represents the quantum confinement property of the nanoparticles. In the quantum confinement range, the band gap of the particle increases as the particle size decreases and results in the shift of absorption edge to lower wavelength.

The XRD pattern was recorded to identify the crystalline structure of the synthesized nanoparticles. Fig. 1(d) represents the XRD pattern of biosynthesized SnO_2 QDs. The biosynthesized SnO_2 QDs were crystalline in nature and the diffraction pattern reveals the tetragonal crystal structure of SnO_2. The biosynthesized material showed peaks at $2\theta=26.3^o$, 33.9^o and 51.5^o. These peaks correspond to (110), (101), and (211) plane, respectively. All the peaks were well indexed to the tetragonal rutile crystal structure of SnO_2 QDs (JCPDS 41-445) [23].

The average crystalline size was calculated from the XRD pattern using Scherrer's equation: $D= k\lambda/\beta Cos\theta$, where D is the average crystallite size, λ is the X-ray wavelength, β is the full width at half maximum, θ is the Bragg angle and k is the so-called shape factor whose value is 0.9 [23]. The average calculated crystalline size of biosynthesized SnO_2 QDs is ~4.6 nm. Therefore, the synthesized SnO_2 nanoparticles fall in the quantum regime. Hence, from the XRD pattern, it is apparent that crystalline SnO_2 quantum dots (QDs) with tetragonal crystal structure were formed using sugar cane juice which acts as complexing as well as capping agent.

RSC Advances Accepted Manuscript

The detailed observations of electron microscopic analysis for biosynthesized SnO_2 QDs were shown in Fig. 2 (a, b and c). The size distribution and morphology of biosynthesized SnO_2 QDs were depicted by TEM and HRTEM images. The TEM and HRTEM images (Fig. 2a, 2b) showed the formation of spherical particles with diameter of ~ 2.5-4.5 nm. The particle size obtained from TEM image is in good agreement with the crystalline size calculated from the XRD data. The spacing between the adjacent lattice fringes calculated from HRTEM image (Fig. 2b) was found to be 0.175 nm apart and corresponds to (211) lattice plane of standard SnO_2. The selected area electron diffraction (SAED) pattern (Fig. 2c) corresponds to the (110), (101) and (211) lattice plane for tetragonal crystal structure of SnO_2 (JCPDS 41-1445) [23]. The lattice planes obtained from the SAED pattern matches well with the XRD results of SnO_2 quantum dots. Hence, TEM images and SAED pattern confirmed the formation of SnO_2 QDs having tetragonal crystal structure.

Fig. 2(d) represents the EDS spectrum of the biosynthesized SnO_2 QDs. The spectrum showed intense peaks of Sn and oxygen at 3.4 eV and 0.5 eV, respectively. The EDS spectrum therefore confirmed the presence of Sn and O. The presence of intense peaks of Sn and O in the EDS spectra clearly indicated the presence of Sn and O only. The EDS analysis also showed the Sn:O composition of 1:2 which was in compliance with the SnO_2 stoichiometry. A signal of chlorine (Cl) and middle-range signals of phosphorus (P) were also recognized. The signals arising for the phophorous and chlorine are due to the presence phosphorous and chlorine in the sugar cane juice [25, 13]. Hence, the peaks of Sn and O in the EDS profile proved the existence of pure SnO_2 nanoparticle.

3.2. Role of Sugar cane juice:

Sugar cane juice contains biomolecules, such as sugar, aminoacids, monosaccharides, disaccharides, polysaccharides and organic acids. It also contains starch and inorganic ions, such as chloride, calcium, phosphorous, etc. [13]. In the biosynthesis of SnO_2 QDs, the biomolecules present in the sugar cane juice

RSC Advances Accepted Manuscript

plays an important role. The biomolecules, such as aminoacids, other organic acids and carbohydrate molecules (viz., monosaccharide, disaccharide and polysaccharides) present in the juice act as complexing and capping agent in the synthesis of SnO_2 QDs. The Sn^{2+} ions form complex with the aminoacids and other organic acids, which on microwave irradiation, break down to form SnO_2 QDs. The rapid explosion of energy through microwave irradiation leads to the formation of SnO_2 QDs.

The biomolecules present in the sugar cane juice also got adsorbed on the surface of SnO_2 quantum dots and thereby act as a good capping agent. Generally, capping agents are used to inhibit nanoparticle overgrowth and aggregation. It also controls the structural characteristics of the resulted nanoparticles. In this case, the biomolecules present in the sugar cane juice act as a complexing as well as capping agent. The biomolecules also act as ligands to form complexes with the precursor metal ion thereby acting as a good complexing agent. When particle growth is concerned, each particle on nucleation started to grow on all directions depending upon the synthesis conditions. In presence of capping agent, i.e., biomolecules present in sugar cane juice, the growth of the nucleated particle is suppressed thereby leading to the formation of SnO_2 QDs. The steric forces keep the nucleated ligands separated from each other and therefore prevent agglomeration. The biosynthesized SnO_2 QDs were capped by the biomolecules, such as carbohydrates, aminoacids and other biomolecules. Therefore, these molecules provide stability to the synthesized SnO_2 QDs and protects from agglomeration. The analysis of FTIR spectrum also depicts the presence of biomolecules, such as aminoacids, organic acids, proteins, monosaccharides, and polysaccharides on the surface of SnO_2 QDs and thereby confirms the role of biomolecules present in the sugar cane juice as capping agent. The FTIR study thus supported the hypothesis of the role of aminoacids, carbohydrates and other biomolecules present in sugar cane juice in the synthesis of SnO_2 QDs. Therefore, in the synthesis of SnO_2 QDs, the biomolecules present in the sugar cane juice act as complexing as well as capping agent.

RSC Advances Accepted Manuscript

3.3. Evaluation of Photocatalytic Activity of biosynthesized SnO_2 QDs:

The photocatalytic activity of the biosynthesized SnO_2 QDs was assessed by monitoring the changes in the optical absorption spectra of RB and MB solution. The degradation process involves photochemical reactions on the surface of the SnO_2 nanoparticles. Hence an increase in the surface area of the photocatalyst leads to a greater degradation of the dye. The size and the dispersion of the photocatalyst in the solution played an important role in the degradation of dye.

Fig. 3(a) depicts the UV-visible spectra for the photodegradation of RB dye using SnO_2 QDs as a photocatalyst under direct sunlight. The UV-visible spectra of the dye show a strong absorption band at 540 nm. The addition of biosynthesized SnO_2 QDs leads to a decrease in the absorption band with irradiation time. The solution becomes colorless within 180 min. This implies the disappearance of the absorption band at 540 nm which indicates complete degradation of the dye.

Fig. 4(a) showed the UV-visible spectra for degradation of MB dye using SnO_2 QDs as a photocatalyst under solar radiation. UV-visible spectra of dye showed a strong absorption band at 663 nm. After the addition of SnO_2 QDs, the absorption band started decreasing with irradiation time. The absorption band at 663 nm almost disappeared within 240 min and the color of the MB solution also fades away. These indicate the destruction of chromophoric structure of MB dye.

The photodegradation reaction followed pseudo first order kinetics and the rate of the reaction can be obtained using the following equation [23]:

$$\ln A_t = - kt + \ln A_o \text{ ------ (2)}$$

where k is the rate constant, A_o and A_t are absorbance or concentration before and after degradation of dye, respectively. The rate constant for photodegradation of RB and MB dye can be calculated using equation (2). Fig. 3(b) and 4(b) represents the plot of $\ln[A_t]$ versus irradiation time (t) for RB and MB dye. The plot gives a linear relationship. Hence, the slope of the line represents the rate constant (k) for the

RSC Advances Accepted Manuscript

photodegradation of RB and MB dye. The value of k is found to be $2.1x10^{-2}$ min^{-1} and $1.0x10^{-2}min^{-1}$ for RB and MB dye, respectively.

The percentage efficiency of photodegradation of RB dye with time was graphically represented in Fig. 3c. It was observed that 99.3% of the dye degraded photochemically within 180 min using biosynthesized SnO_2 QDs. Fig. 4(c) represented the percentage efficiency of photocatalytic degradation of MB dye with time. It was evident that 96.8% of MB dye degraded photochemically within 240 min by solar irradiation using biosynthesized SnO_2 QDs.

The photodegradation of RB and MB dyes were carried out using commercial SnO_2 in order to compare the photocatalytic activity of SnO_2 QDs with commercial SnO_2. The progress of the reactions was similarly investigated by recording UV-visible spectra at regular interval of time. Fig. 5(a, c) represents the absorption spectra for the photodegradation of RB and MB dye using commercial SnO_2, respectively. The photodegradation reaction follows pseudo first order kinetics and the slope obtained from the plot of ln A_t versus irradiation time (t) for RB and MB dye (Fig. 5b and 5d) represents the rate constant. The degradation rate constant for RB and EY dye were found to be $0.48x10^{-2}$ min^{-1} and $0.23x10^{-2}$ min^{-1}, respectively. The percentage efficiency for photodegradation of RB and MB dye were displayed graphically in Fig. 5(e, f). From the graph, it was apparent that ~83.9% of RB dye was degraded within 420 min and about 56.8 % of MB degraded within 360 min.

The comparison of photocatalytic activity of the synthesized SnO_2 QDs with that of commercial SnO_2 was shown in Table 1. It was evident that the rate of degradation of RB and MB dyes using SnO_2 QDs as a photocatalyst was higher than that of commercial SnO_2. It was also evident that the percentage efficiency of photodegradation of RB and MB dye increases when SnO_2 QDs are introduced as a photocatalyst instead of commercial SnO_2. This was attributed to the fact that with a decrease in the dimensions of SnO_2 QDs, the surface area increases to a great extent which enhances the catalytic properties of SnO_2. Hence,

RSC Advances Accepted Manuscript

the synthesized SnO_2 QDs enhanced the photocatalytic activity to a larger extent as compared to that of commercial SnO_2.

To confirm the photocatalytic activity of biosynthesized SnO_2 QDs, a control experiment was carried out with the two different dye solutions (RB and MB) and irradiated with sunlight in the absence of SnO_2 QDs. It was observed that both the dyes don't undergo degradation. This also experimentally proves the visible light activity of the synthesized SnO_2 QDs. For further assurance, the two different dye solutions (RB and MB) were treated with SnO_2 QDs in the absence of sunlight (dark) and it was evident that both the dye undergoes negligible degradation.

In order to investigate the role of SnO_2 QDs in the photodegradation of RB and MB dyes, the SnO_2 QDs was recovered by simple filtration and washed with hot water and ethanol. The FTIR spectrum of the recovered SnO_2 QDs was recorded. The spectrum doesn't show any change with respect to the earlier spectrum recorded for the synthesized SnO_2 QDs. This evidence proves the stability of synthesized SnO_2 QDs as photocatalyst in the degradation of rose bengal and methylene blue dyes. This also depicts the ultimate fate of SnO_2 QDs as photocatalyst in the degradation reaction.

To confirm the catalytic activity of synthesized SnO_2 QDs, the absorption spectra were also recorded in presence of dye molecules after the complete degradation process. It was evident that the UV-visible spectra of SnO_2 QDs remain unchanged in presence of dye molecules. Therefore, SnO_2 QDs act as a catalyst in the degradation of dye and so no interaction occurs between the catalyst and dye molecules. For further confirmation, XRD pattern of the recovered SnO_2 QDs were also recorded and no changes were observed in their respective peak positions. These evidences proved the role of SnO_2 QDs as photocatalyst in the degradation of RB and MB dyes.

3.4. Mechanism for photodegradation of Rose Bengal (RB) and Methylene Blue (MB) dye:

RSC Advances Accepted Manuscript

On illumination of the catalyst surface (SnO_2 QDs) with light energy higher than its band-gap energy, leads to the formation of holes (h+) in the valence band and an electron (e-) in the conduction band of SnO_2 QDs. The holes (h+) act as an oxidizing agent and oxidize the pollutant directly or react with water to form hydroxyl radicals. The electron (e-) in the conduction band acts as a reducing agent and reduces the oxygen adsorbed on the surface of SnO_2 photocatalyst. The probable mechanism for the photodegradation of RB dye using SnO_2 photocatalyst can be depicted as [22]:

$$SnO_2 + h\nu \rightarrow e^- + h^+$$

$$H_2O + h^+ \rightarrow OH^- + H^+$$

$$OH^- + h^+ \rightarrow {}^{\bullet}OH$$

$$e^- + O_2 \rightarrow {}^{\bullet}O_2^-$$

$${}^{\bullet}O_2^- + H^+ \rightarrow {}^{\bullet}OOH$$

$$RB + h\nu \rightarrow RB^*$$

$$RB^* + SnO_2 \rightarrow RB + SnO_2\,(e^-)$$

$$SnO_2\,(e^-) + O_2 \rightarrow SnO_2 + O_2^-$$

$$SnO_2\,(e^-) + {}^{\bullet}O_2^- + H^+ \rightarrow SnO_2 + H_2O_2$$

$$SnO_2\,(e^-) + H_2O_2 \rightarrow SnO_2 + {}^{\bullet}OH + OH^-$$

$$h^+ + RB \rightarrow \text{degradation products}$$

RSC Advances Accepted Manuscript

$$RB^{*} + O_2 \text{ or } {}^{\bullet}OH \text{ or } {}^{\bullet}O_2^{-} \rightarrow \text{degradation products}$$

The probable mechanism for the photocatalytic degradation of MB can be schematically visualized as [22]:

$$SnO_2 + h\nu \rightarrow e^{-} + h^{+}$$

$$H_2O + h^{+} \rightarrow OH^{-} + H^{+}$$

$$OH^{-} + h^{+} \rightarrow {}^{\bullet}OH$$

$$e^{-} + O_2 \rightarrow {}^{\bullet}O_2^{-}$$

$${}^{\bullet}O_2^{-} + H^{+} \rightarrow {}^{\bullet}OOH$$

$$MB + h\nu \rightarrow MB^{*}$$

$$MB^{*} + SnO_2 \rightarrow MB + SnO_2\,(e^{-})$$

$$SnO_2\,(e^{-}) + O_2 \rightarrow SnO_2 + O_2^{-}$$

$$SnO_2\,(e^{-}) + {}^{\bullet}O_2^{-} + H^{+} \rightarrow SnO_2 + H_2O_2$$

$$SnO_2\,(e^{-}) + H_2O_2 \rightarrow SnO_2 + {}^{\bullet}OH + OH^{-}$$

$$h^{+} + MB \rightarrow \text{degradation products}$$

$$MB^{*} + O_2 \text{ or } {}^{\bullet}OH \text{ or } {}^{\bullet}O_2^{-} \rightarrow \text{degradation products}$$

RSC Advances Accepted Manuscript

The excited dye injects an electron to the conduction band of SnO_2 and it is scavenged by pre-adsorbed oxygen (O_2) to form active oxygen radicals. These active radicals drive the photodegradation process. The SnO_2 QDs played a significant role as an electron carrier. Such assisted photo process provides an attractive route to treat dye pollutants using sunlight and shown in scheme 1.

RSC Advances Accepted Manuscript

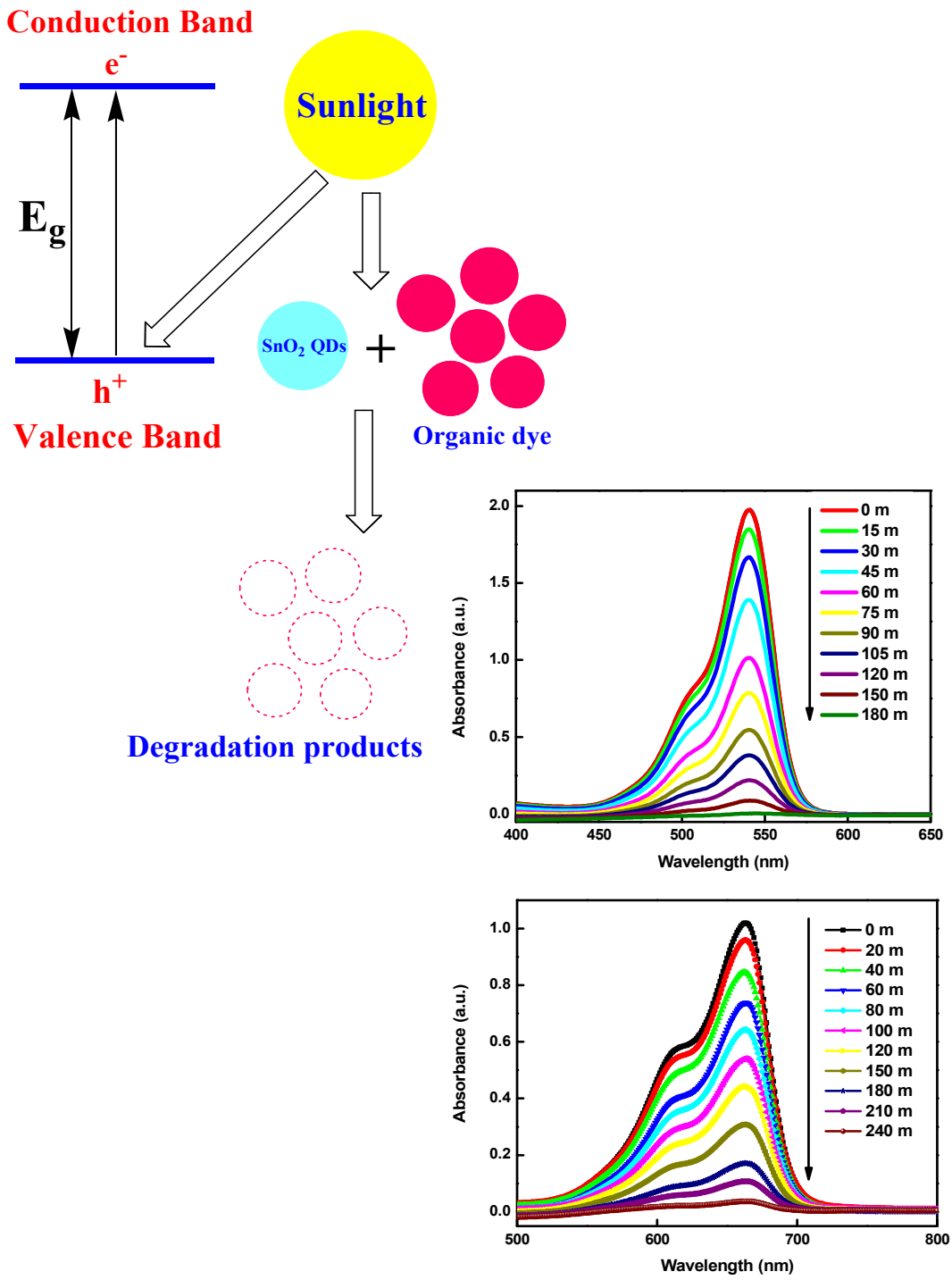

Scheme 1. Schematic representation of photodegradation of RB and MB dye using SnO_2 QDs.

RSC Advances Accepted Manuscript

3.5. Catalytic Reduction of p-nitro phenol to p-amino phenol:

The catalytic efficiency of SnO_2 QDs was examined by carrying out the reduction of PNP to PAP in aqueous medium using $NaBH_4$. Absorption spectra of p-nitrophenol showed λ_{max} at 317 nm in aqueous medium (Fig. 6a). The subsequent addition of freshly prepared $NaBH_4$ solution to PNP leads to a red shift from 317 nm to 403 nm (Fig. 6b). The color of the solution changes to intense yellow with addition of $NaBH_4$. This is because of the formation of 4-nitrophenolate ions under alkaline condition [22]. The peak obtained at 403 nm remained unaltered after a couple of days in absence of any catalyst.

The yellow color of PNP solution slowly faded after the addition of 300µl of 0.01g of SnO_2 QDs and finally disappeared on complete reduction of PNP. This was monitored by UV-visible spectroscopy at a regular interval of time. Fig. 6(c) showed the UV-visible spectra for the reduction of PNP. It is evident from Fig. 6(c) that the characteristic peak for PNP decreases with time with the addition of SnO_2 nanocatalyst and there is a simultaneous appearance of a new peak centered at 297 nm. This is due to the reduction of PNP into PAP. The peak at 297nm increases gradually with time due to the formation of PAP [22]. The complete reduction of PNP takes place within 60 min. Hence, SnO_2 QDs act as an efficient catalyst in the reduction of PNP in presence of $NaBH_4$. Generally, most of the reactions followed pseudo-first order kinetics [22], but in some cases zero-order kinetics were also reported in the literature [26]. However, in our case the reaction followed pseudo-first order kinetics [22]. The rate constant (k) has been determined from the linear plot of ln $[A_t]$ versus reduction time and found to be 3.3×10^{-2} min^{-1} (Fig. 6d). About 99.5% of p-nitrophenol was reduced to p-amino phenol using $NaBH_4$ in presence of SnO_2 QDs as catalyst.

RSC Advances Accepted Manuscript

3.6. Mechanism of reduction of p-nitro phenol to p-amino phenol using biosynthesized SnO_2 QDs as catalyst:

The mechanistic pathway for the hydrogenation of p-nitrophenol involves the following steps: (i) Adsorption of hydrogen, (ii) Adsorption of p-nitrophenol into metal-oxide surface, (iii) electron transfer mediated by metal-oxide surface from BH_4^- ion to p-nitophenol and (iv) desorption of p-aminophenol. The electron is transferred from donor BH_4^- ion in the reduction of p-nitrophenol. In presence of SnO_2 QDs, BH_4^- ion gets adsorbed on its surface and discharge of electrons from BH_4^- ion takes place through metal oxide to the acceptor i.e., p-nitrophenol. The aqueous medium provides the required amount of H^+ ion for complete reduction of p-nitrophenol into p-aminophenol [27]. The probable mechanism can be schematically represented as follows:

$$NaBH_4 + 4H_2O \xrightarrow{SnO_2\ QDs} NaB(OH)_4 + 4H_2$$

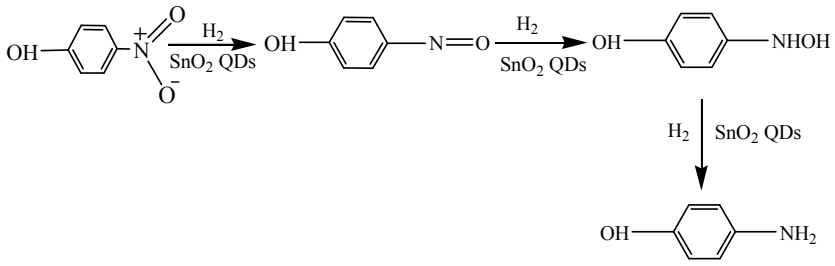

4. Conclusion

In this article, a green, eco-friendly, environmentally benign, facile and cost-effective synthesis of SnO_2 QDs was developed by microwave heating method using sugar cane juice. The biomolecules present in the sugar cane juice act as complexing as well as capping agent in the synthesis of SnO_2 QDs. The TEM, HRTEM images and SAED pattern showed the formation of well crystalline, spherical SnO_2 QDs with an average particle size of ~2.5-4.5 nm. XRD and SAED pattern revealed the tetragonal rutile crystalline structure of SnO_2 QDs. A significant blue shift was observed in the band gap energy of synthesized SnO_2 QDs (4.1 eV) from bulk SnO_2 (3.6 eV) due to quantum effect. The synthesized SnO_2 QDs also act as an

RSC Advances Accepted Manuscript

efficient photocatalyst in the degradation of Rose Bengal and Methylene blue dyes by solar radiation. The catalytic activity of biosynthesized SnO_2 QDs was also evaluated by the reduction of p-nitrophenol in presence of $NaBH_4$ in aqueous medium. About 99.5% of p-nitrophenol was reduced within 60 min by $NaBH_4$ in presence of SnO_2 QDs as catalyst. This also showed that the synthesized SnO_2 QDs act as an efficient catalyst in the reduction of p-nitrophenol to p-aminophenol.

Acknowledgement

We, the authors, express our heartfelt thanks and gratitude to the Director, NIT Silchar and TEQIP-II for providing lab facilities and scholarship. Our special thanks are extended to NEHU, IIT Bombay and CSMCRI for providing TEM, IR and XRD data.

References:

1. Yeow, S. C.; Ong, W. L.; Wong, A. S. W.; Ho, G. W. Template-free Synthesis and Gas Sensing Properties of Well-controlled Porous Tin oxide Nanospheres. *Sens. Actuators B* **2009,** 143, 295-301.

2. Kansal, S. K.; Singh, M.; Sud, D. Studies on Photodegradation of two Commercial Dyes in Aqueous Phase Using Different Photocatalysts. *J. Hazard. Mater.* **2007,** 141, 581-590.

3. Carreno, N. L. V.; Fajardo, H. V.; Maciel, A. P.; Valentini, A.; Pontes, F. M.; Probst, L. F. D.; Leite, E. R.; Longo, E. Selective Synthesis of Vinyl Ketone Over SnO_2 Nanoparticle Catalysts Doped with Rare Earths. *J. Mol. Catal. A: Chem.* **2004,** 207, 91-96.

4. Li, F.; Xu, J.; Yu, X.; Chen, L.; Zhu, J.; Yang, Z.; Xin, X. One-step Solid-state Reaction Synthesis and Gas Sensing Property of Tin oxide Nanoparticles. *Sens. Actuators B* **2002,** 81, 165- 169.

5. Shang, G.; Wu, J.; Huang, M.; Lin, J.; Lan, Z.; Huang, Y.; Fan, L. Facile Synthesis of Mesoporous Tin Oxide Spheres and Their Applications in Dye-Sensitized Solar Cells. *J. Phys. Chem. C* **2012,** 116, 20140-20145.

RSC Advances Accepted Manuscript

6. Han, S.; Jang, B.; Kim, T.; Oh S. M.; Hyeon, T. Simple Synthesis of Hollow Tin Dioxide Microspheres and Their Application to Lithium-ion Battery Anodes. *Adv. Funct. Mater.* **2005,** 15, 1845-1850.

7. Meduri, P.; Pendyala, C.; Kumar, V.; Sumanasekera, G. U.; Sunkara, M. K. Hybrid Tin Oxide Nanowires as Stable and High Capacity Anodes for Li-Ion Batteries. *Nano Lett.* **2009,** 9, 612-616.

8. Gu, F.; Wang, S.; Cao, H.; Li, C. Synthesis and Optical Properties of SnO_2 Nanorods. *Nanotechnology* **2008,** 19, 095708.

9. Singh, M.K.; Mathpal, M.C.; Agarwal, A. Optical Properties of SnO_2 Quantum Dots Synthesized by Laser Ablation in Liquid. *Chem. Phys. Lett.,* 2012, 536, 87-91.

10. Pang, G.; Chen, S.; Koltypin, Y.; Zaban, A.; Feng, S.; Gedanken, A. Controlling the Particle Size of Calcined SnO_2 Nanocrystals. *Nano Lett.* **2001,** 1, 723-726.

11. Xiao, L.; Shen, H.; Hagen, R.V.; Pan, J.; Belkoura, L.; Mathur, S. Microwave Assisted Fast and Facile Synthesis of SnO_2 Quantum Dots and Their Printing Applications. *Chem. Commun.,* **2010,** 46, 6509-6511.

12. Srivastava, N.; Mukhopadhyay, M. Biosynthesis of SnO_2 Nanoparticles Using Bacterium *Erwinia herbicola* and Their Photocatalytic Activity for Degradation of Dyes. *Ind. Eng. Chem. Res.* **2014,** 53, 13971−13979.

13. Walford, S. N. Composition of cane juice. *Proc. S. Afr. Sug. Technol. Ass.* **1996,** 70, 265 – 266.

14. Pal, J.; Deb, M. K.; Deshmukh, D. K.; Sen, B. K. Microwave-assisted Synthesis of Platinum Nanoparticles and Their Catalytic Degradation of Methyl Violet in Aqueous Solution. *Appl. Nanosci.* **2014,** 4, 61-65.

RSC Advances Accepted Manuscript

15. Sangami, G.; Dharmaraj, N. UV-visible Spectroscopic Estimation of Photodegradation of Rhodamine-B Dye Using Tin(IV) Oxide Nanoparticles. *Spectrochim. Acta. A. Mol. Biomol. Spectrosc.* **2012,** 97, 847-852.

16. Linsebigler, A. L.; Lu, G.; Yates, J. T. Photocatalysis on TiO_2 Surfaces: Principles, Mechanisms, and Selected Results. *Chem. Rev.* **1995,** 95, 735−758.

17. Jianga, W.; Joens, J. A.; Dionysioub, D. D.; O'Shea, K. E. Optimization of Photocatalytic Performance of TiO_2 Coated Glass Microspheres Using Response Surface Methodology and the Application for Degradation of Dimethyl Phthalate. *J. Photochem. Photobiol. A: Chem.* **2013,** 262, 7-13.

18. Qin, H.; Li, W.; Xia, Y.; He, T. Photocatalytic Activity of Heterostructures Based on ZnO and N-doped ZnO. *ACS Appl. Mater. Interfaces.* **2011,** 3, 3152−3156.

19. Liu, L.; Li, Y.; Yuan, S. M.; Ge, M.; Ren, M. M.; Sun, C. S.; Zhou, Z. Nanosheet-Based NiO Microspheres: Controlled Solvothermal Synthesis and Lithium Storage Performances. *J. Phys. Chem. C,* **2010,** 114, 251−255.

20. Mao, C. J.; Pan, H. C.; Wu, X. C.; Zhu, J. J.; Chen, H. Y. Sonochemical Route for Self-assembled V_2O_5 Bundles with Spindle-like Morphology and Their Novel Application in Serum Albumin Sensing. *J. Phys. Chem. B,* **2006,** 110, 14709−14713.

21. Ahmaruzzaman, M.; Gayatri, S. L. Batch Adsorption of 4-Nitrophenol by Acid Activated Jute Stick Char: Equilibrium, Kinetic and Thermodynamic Studies. *Chem. Eng. J.* **2010,** 158, 173-180.

22. Mandlimath, T.R.; Gopal, B. Catalytic Activity of First Row Transition Metal Oxides in the Conversion of p-Nitrophenol to p-Aminophenol. *J. Mol. Catal. A: Chem.* **2011,** 350, 9-15.

23. Bhattacharjee, A.; Ahmaruzzaman, M.; Sinha, T. Surfactant Effects on the Synthesis of Durable Tin-oxide Nanoparticles and Its Exploitation as a Recyclable Catalyst for Elimination of Toxic Dye: A Green and Efficient Approach for Wastewater Treatment. *RSC Adv.* **2014,** 4, 51418-51429.

RSC Advances Accepted Manuscript

24. Saha, N. K.; Balakrishnan, M.; Ulbricht, M. Sugarcane Juice Ultrafiltration: FTIR & SEM Analysis of Polysaccharide Fouling. *J. Membr. Sci.* **2007,** 306, 287-297.

25. Kulkarni, A. A.; Bhanage, B. M. Ag@AgCl Nanomaterial Synthesis Using Sugar Cane Juice and Its Application in Degradation of Azo Dyes. *ACS Sustainable Chem. Eng.* **2014,** 2, 1007-1013.

26. Saha, S.; Pal, A.; Kundu, S.; Basu, S.; Pal, T. Photochemical Green Synthesis of Calcium-Alginate-Stabilized Ag and Au Nanoparticles and Their Catalytic Application to 4-Nitrophenol Reduction. *Langmuir* **2010,** 26, 2885-93.

27. Tamuly, C.; Saikia, I.; Hazarika, M.; Das, M. R. Reduction of Aromatic Nitro Compounds Catalyzed by Biogenic CuO Nanoparticles. *RSC Adv.* **2014,** 4, 53229-36.

Figure:

1. **(a)** FT-IR spectra of biosynthesized SnO_2 QDs, **(b)** Absorption spectra of biosynthesized SnO_2 QDs (0.01M), **(c)** Plot of $(\alpha h\nu)^2$ versus incident photon energy ($h\nu$) for biosynthesized SnO_2 QDs, **(d)** XRD pattern of biosynthesized SnO_2 QDs.

2. **(a)** TEM microphotograph of biosynthesized SnO_2 QDs, **(b)** HRTEM image of biosynthesized SnO_2 QDs**, (c)** SAED pattern of biosynthesized SnO_2 QDs, **(d)** EDS spectrum of biosynthesized SnO_2 QDs.

3. **(a)** Photodegradation of Rose Bengal (RB) dye by solar irradiation using biosynthesized SnO_2 QDs as photocatalyst, **(b)** Plot of $\ln(A_t)$ versus irradiation time, t, for photodegradation of Rose Bengal (RB) dye using biosynthesized SnO_2 QDs as photocatalyst, **(c)** Percentage efficiency of photodegradation of Rose Bengal (RB) dye with time (error bars represent standard deviation of triplicate experiments)

4. **(a)** Photodegradation of Methylene Blue (MB) dye by solar irradiation using SnO_2 QDs as photocatalyst **(b)** Plot of $\ln(A_t)$ versus irradiation irradiation time, t, for photodegradation of Methylene

RSC Advances Accepted Manuscript

Blue (MB) dye using SnO_2 QDs as photocatalyst, **(c)** Percentage efficiency of photodegradation of Methylene Blue (MB) dye with time (error bars represent standard deviation of triplicate experiments)

5. **(a)** Photodegradation of Rose Bengal (RB) dye by solar irradiation using commercial SnO_2 as photocatalyst, **(b)** Plot of $\ln(A_t)$ versus irradiation irradiation time, t, for photodegradation of Rose Bengal (RB) dye using commercial SnO_2 as photocatalyst, **(c)** Photodegradation of Methylene blue (MB) dye by solar irradiation using commercial SnO_2 as photocatalyst, **(d)** Plot of $\ln(A_t)$ versus irradiation time, t, for photodegradation of Methylene blue (MB) dye using commercial SnO_2 as photocatalyst, **(e)** Percentage efficiency of photodegradation of Rose Bengal (RB) dye using commercial SnO_2 as photocatalyst with time, **(f)** Percentage efficiency of photodegradation of Methylene blue (MB) dye using commercial SnO_2 as photocatalyst with time.

6. **(a)** Absorption spectra of 60µl (6.00×10^{-3} M) p-nitro phenol in aqueous medium, **(b)** UV-visible spectra of 60µl (6.00×10^{-3} M) p-nitro phenol + 350 µl (0.1M) $NaBH_4$ in aqueous solution, **(c)** Absorption spectra for reduction of p-nitro phenol by $NaBH_4$ in aqueous medium in presence of biosynthesized SnO_2 QDs as catalyst, **(d)** Plot of $\ln[A_t]$ versus time required for the reduction of p-nitro phenol using SnO_2 QDs as catalyst in presence of $NaBH_4$ in aqueous medium.

RSC Advances Accepted Manuscript

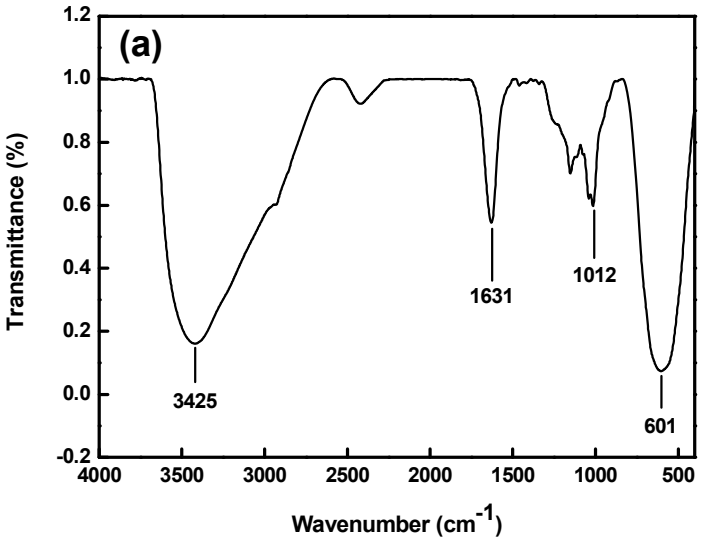

Fig 1. (a) FT-IR spectra of biosynthesized SnO_2 QDs

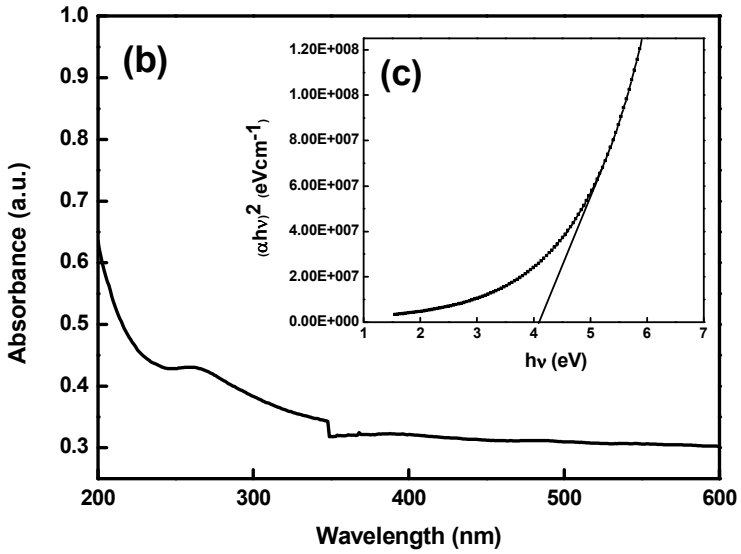

Fig. 1(b) Absorption spectra of biosynthesized SnO_2 QDs (0.01M). Fig. 1(c) Plot of $(\alpha h\nu)^2$ versus incident photon energy (hν) for biosynthesized SnO_2 QDs.

RSC Advances Accepted Manuscript

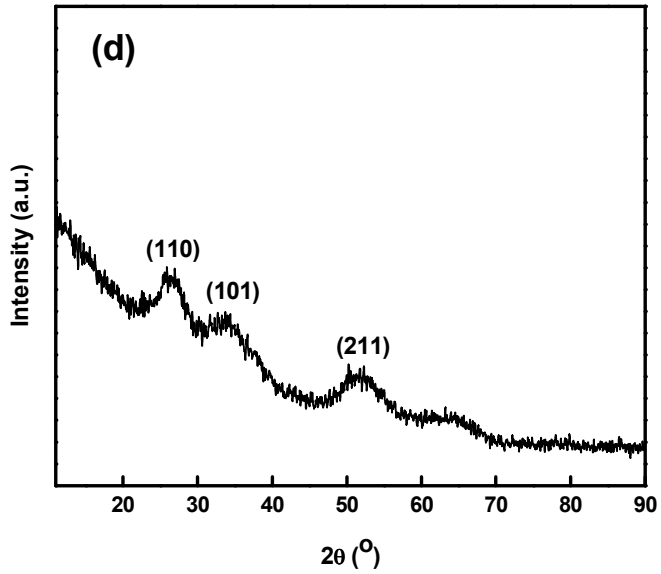

Fig. 1 (d) XRD pattern of biosynthesized SnO_2 QDs.

RSC Advances Accepted Manuscript

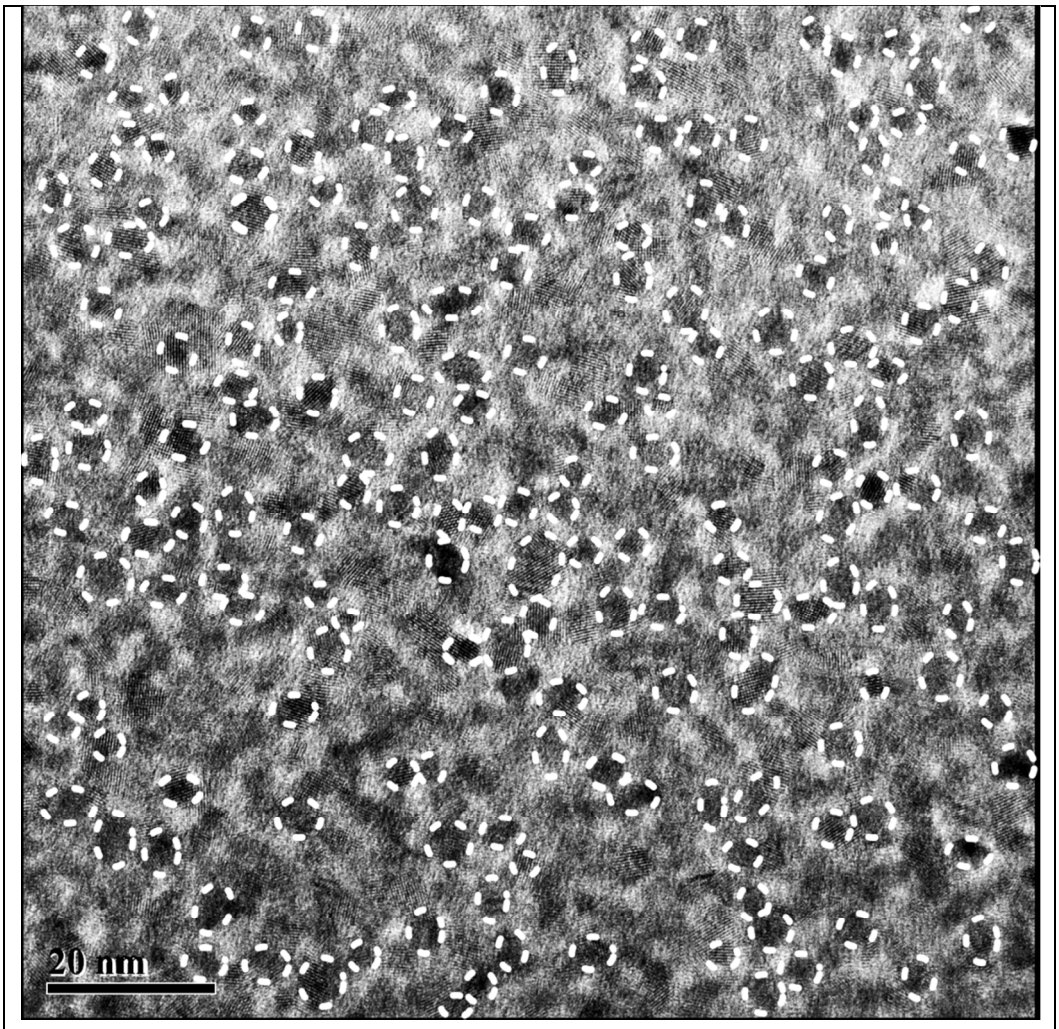

Fig 2. (a) TEM microphotograph of biosynthesized SnO_2 QDs

RSC Advances Accepted Manuscript

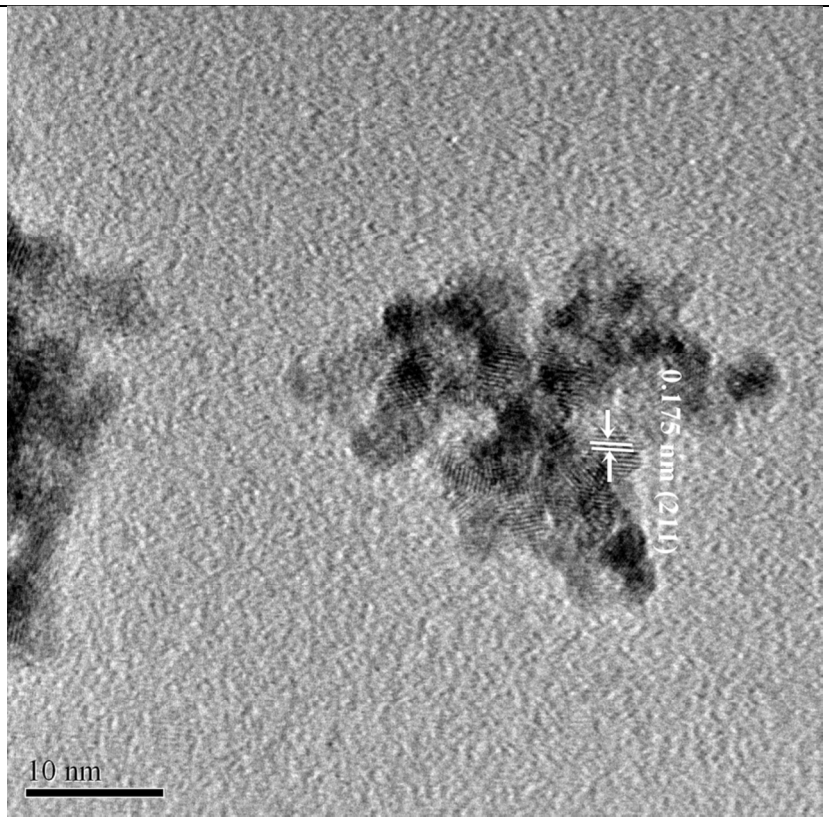

Fig. 2(b) HRTEM image of biosynthesized SnO_2 QDs

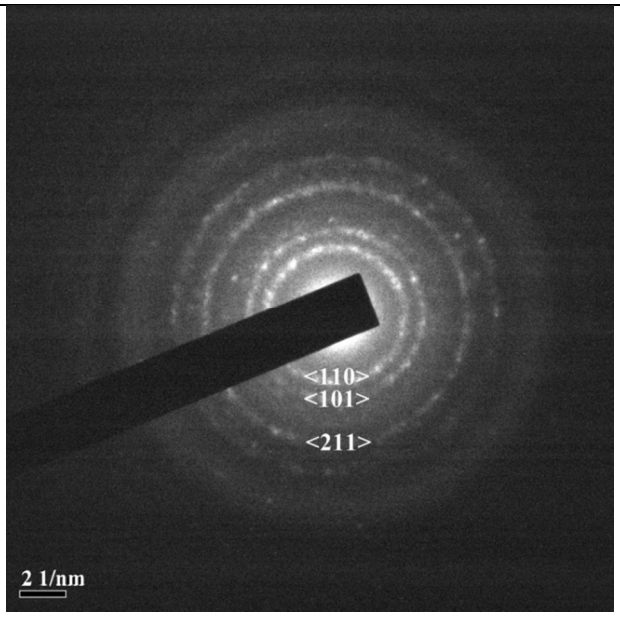

Fig. 2(c) SAED pattern of biosynthesized SnO_2 QDs

RSC Advances Accepted Manuscript

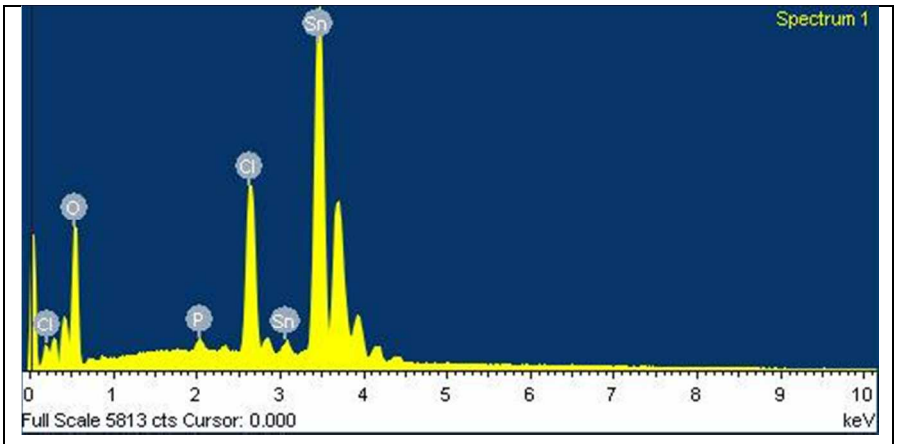

Fig. 2(d) EDS spectrum of biosynthesized SnO_2 QDs

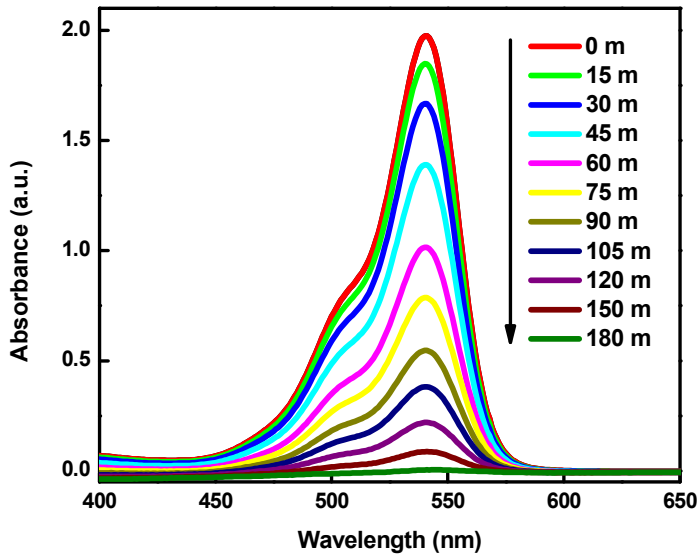

Fig. 3 (a) Photodegradation of Rose Bengal (RB) dye by solar irradiation using biosynthesized SnO_2 QDs as photocatalyst.

RSC Advances Accepted Manuscript

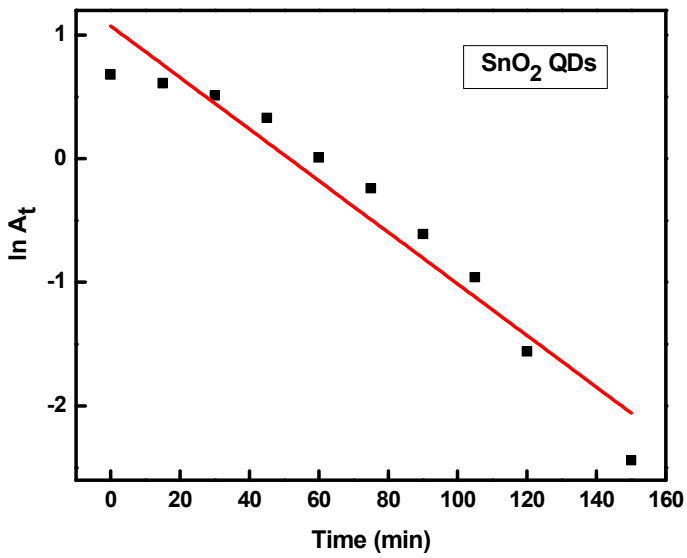

Fig. 3 (b) Plot of ln[A_t] versus irradiation time, t, for photodegradation of Rose Bengal (RB) dye using biosynthesized SnO_2 QDs as photocatalyst.

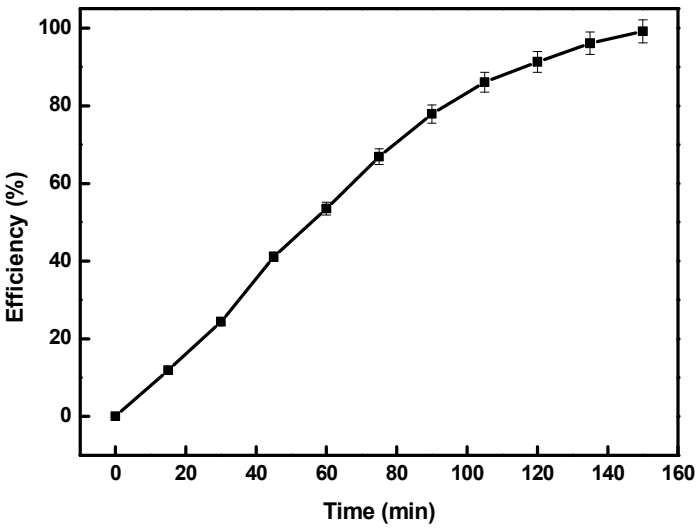

Fig. 3 (c) Percentage efficiency of photodegradation of Rose Bengal (RB) dye with time. Error bars represent standard deviation of triplicate experiments.

RSC Advances Accepted Manuscript

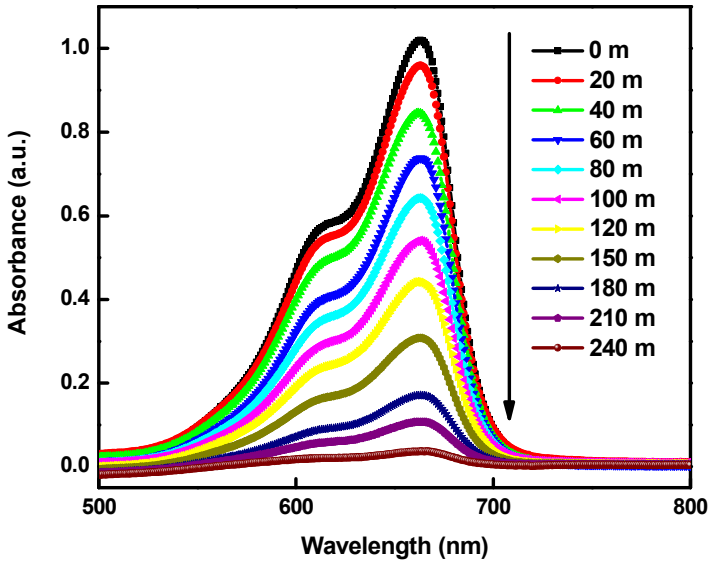

Fig. 4(a) Photodegradation of MB dye by solar irradiation using biosynthesized SnO_2 QDs as photocatalyst.

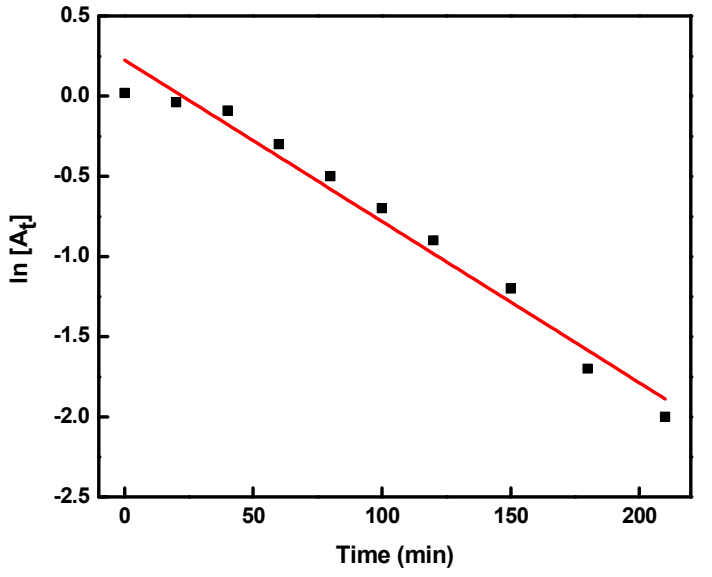

Fig. 4(b) Plot of ln[A_t] versus irradiation irradiation time, t, for photodegradation of MB dye using biosynthesized SnO_2 QDs as photocatalyst.

RSC Advances Accepted Manuscript

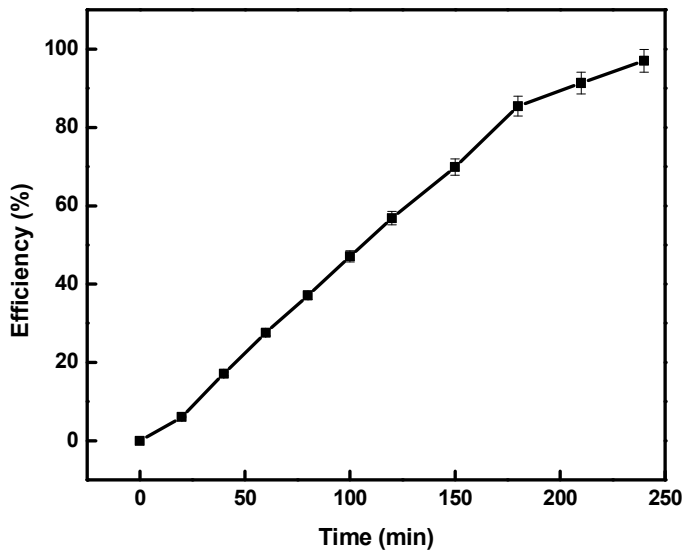

Fig. 4(c) Percentage efficiency of photodegradation of MB with time. Error bars represent standard deviation of triplicate experiments.

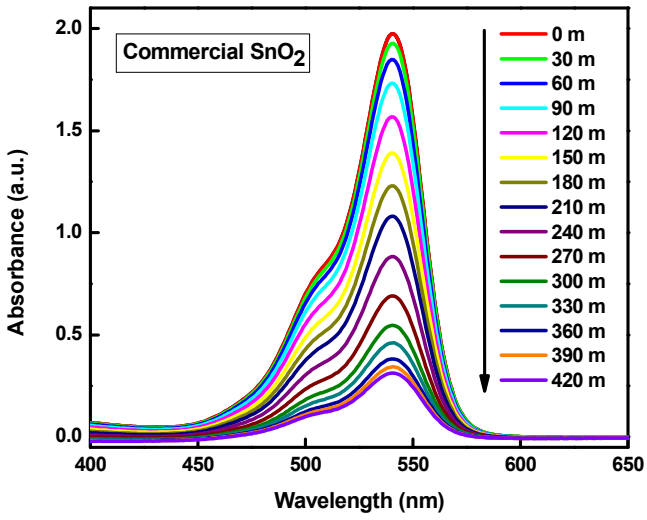

Fig. 5(a) Photodegradation of Rose Bengal (RB) dye by solar irradiation using commercial SnO_2 as photocatalyst

RSC Advances Accepted Manuscript

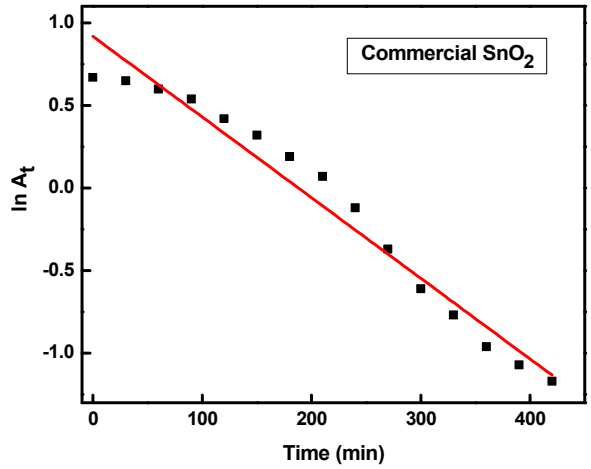

Fig. 5(b) Plot of ln(A_t) versus irradiation time, t, for photodegradation of Rose Bengal (RB) dye using commercial SnO_2 as photocatalyst.

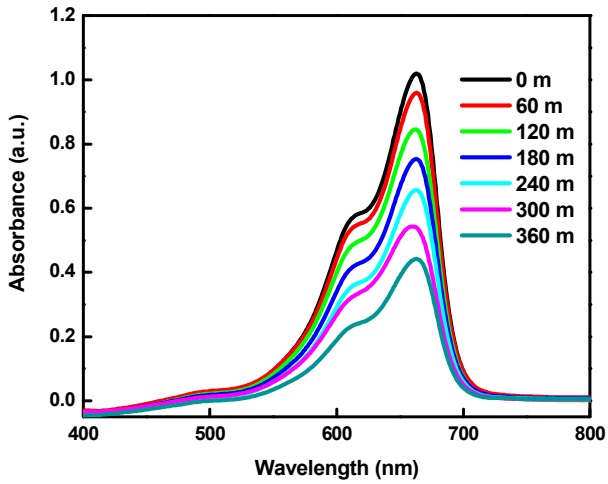

Fig. 5(c) Photodegradation of Methylene blue (MB) dye by solar irradiation using commercial SnO_2 as photocatalyst.

RSC Advances Accepted Manuscript

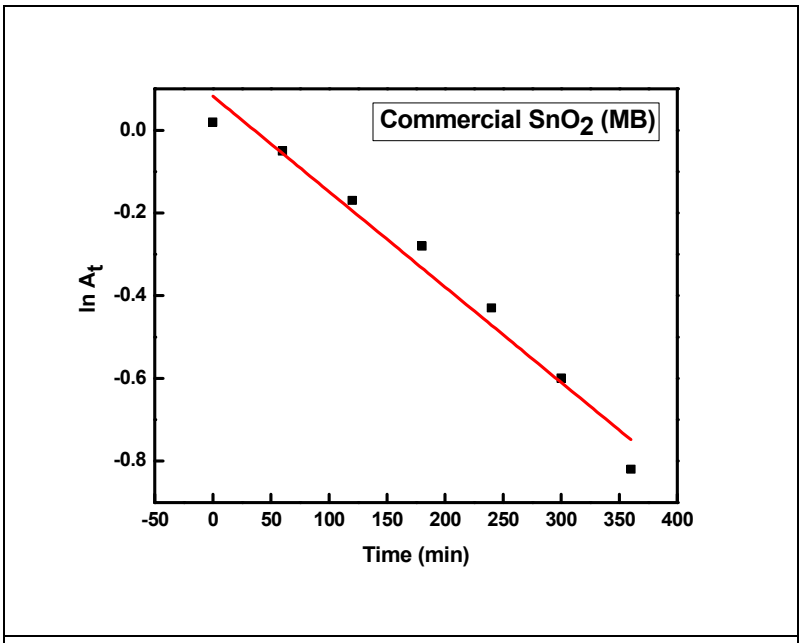

Fig. 5(d) Plot of ln(A_t) versus irradiation time, t, for photodegradation of Methylene blue (MB) dye using commercial SnO_2 as photocatalyst.

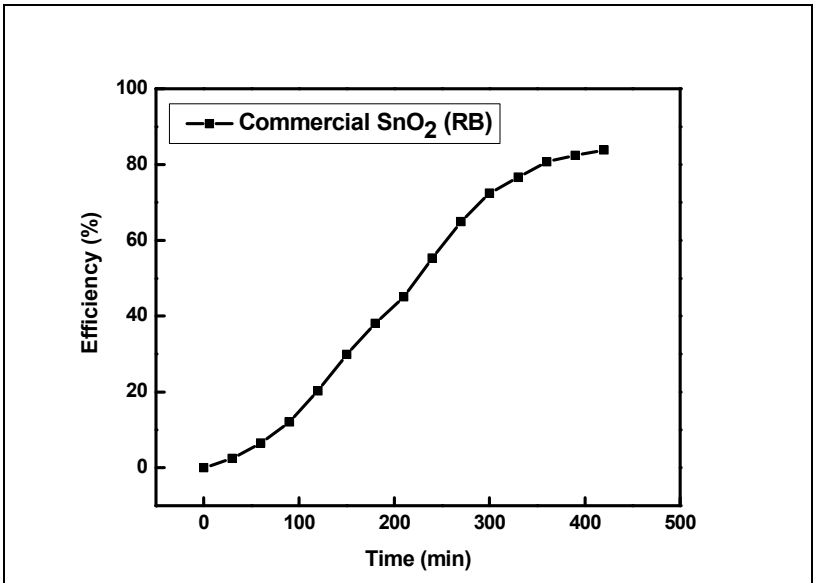

Fig. 5(e) Percentage efficiency of photodegradation of Rose Bengal (RB) dye using commercial SnO_2 as photocatalyst with time

RSC Advances Accepted Manuscript

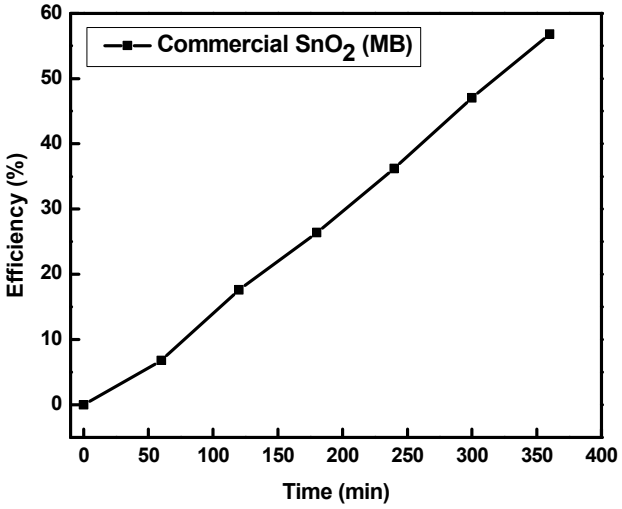

Fig. 5(f) Percentage efficiency of photodegradation of Methylene blue (MB) dye using commercial SnO_2 as photocatalyst with time

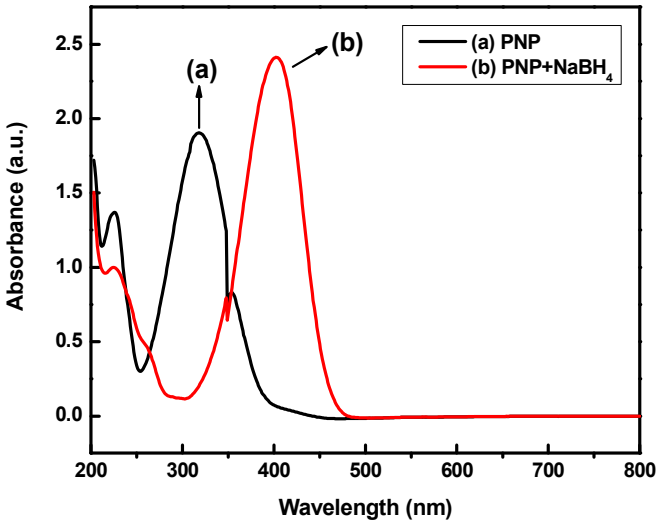

Fig. 6(a) Absorption spectra of 60µl (6.00×10^{-3} M) p-nitro phenol in aqueous medium, (b) UV-visible spectrum of 60µl (6.00×10^{-3} M) p-nitro phenol + 350 µl (0.1M) $NaBH_4$ in aqueous solution.

RSC Advances Accepted Manuscript

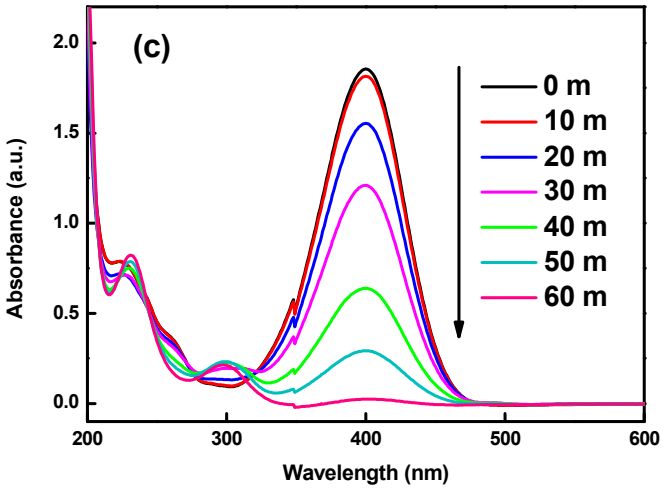

Fig. 6(c) Absorption spectra for reduction of p-nitro phenol by $NaBH_4$ in aqueous medium in presence of biosynthesized SnO_2 QDs as catalyst.

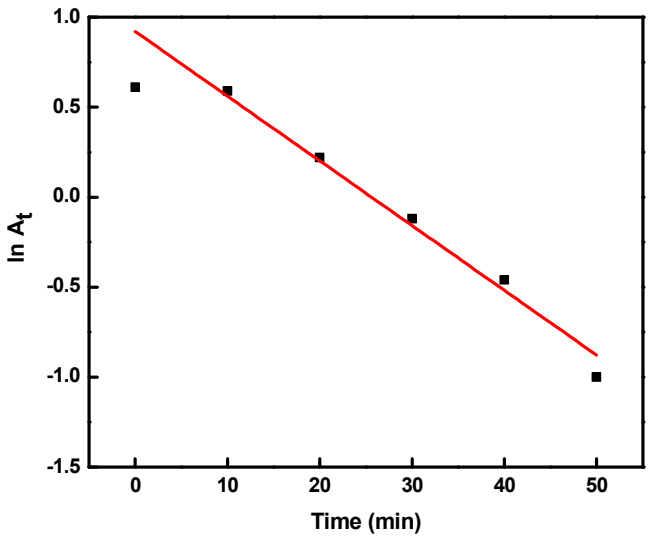

Fig. 6(d) Plot of ln[A_t] versus time required for the reduction of p-nitro phenol using SnO_2 QDs as catalyst in presence of $NaBH_4$ in aqueous medium.

RSC Advances Accepted Manuscript

Table 1. Comparison of results obtained for the photodegradation of Rose Bengal (RB) and Methylene blue (MB) dye using SnO_2 QDs and commercial SnO_2 as photocatalyst.

Dye Degraded	Photocatalyst	Amount added (mg)	Time (min.)	Efficiency (%)	Rate (min^{-1})
Rose Bengal (RB)	SnO_2 QDs	10	180	99.3	2.1×10^{-2}
	Commercial SnO_2	10	420	83.9	0.48×10^{-2}
Methylene blue (MB)	SnO_2 QDs	10	240	96.8	1.0×10^{-2}
	Commercial SnO_2	10	360	56.8	0.23×10^{-2}

RSC Advances Accepted Manuscript

GRAPHICAL ABSTRACT:

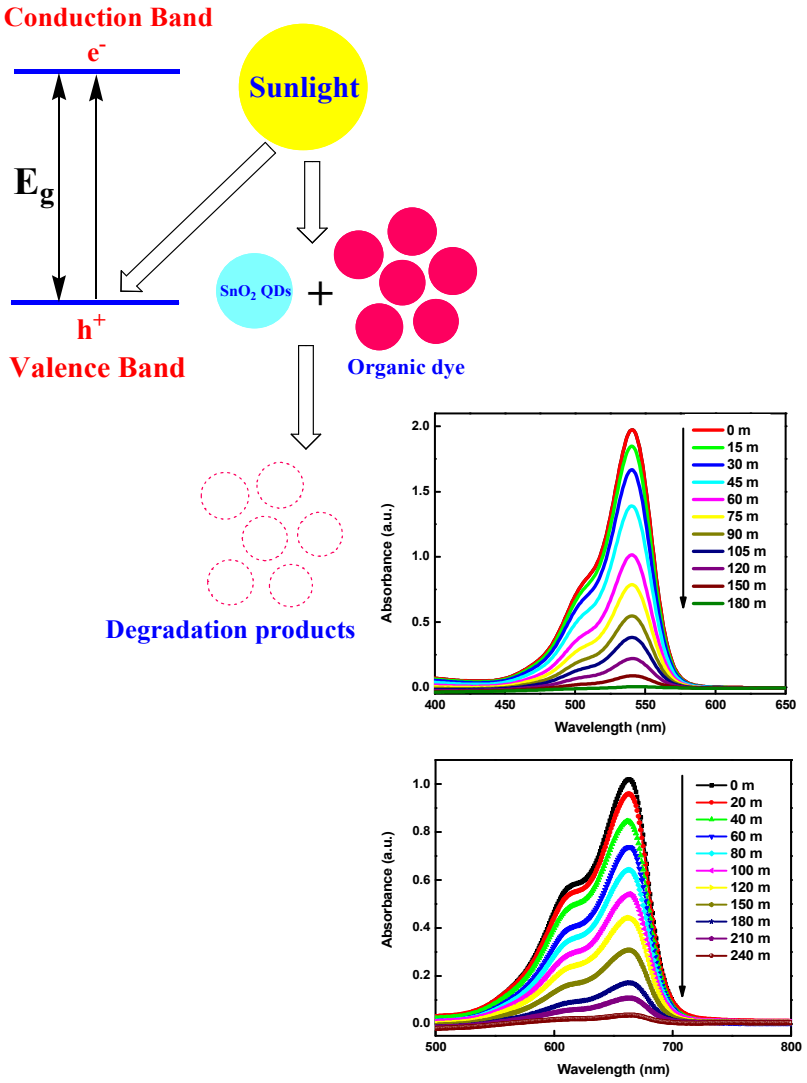

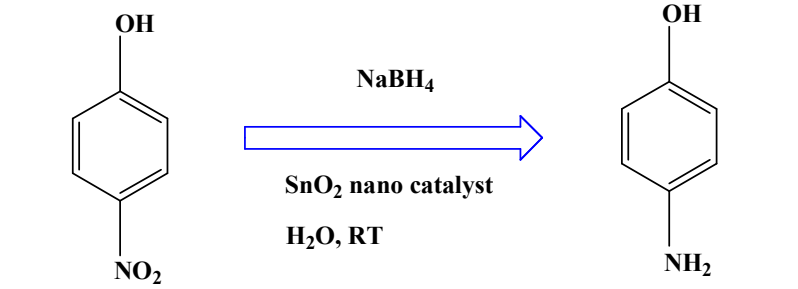

p- nitrophenol **p-aminophenol**

RSC Advances Accepted Manuscript